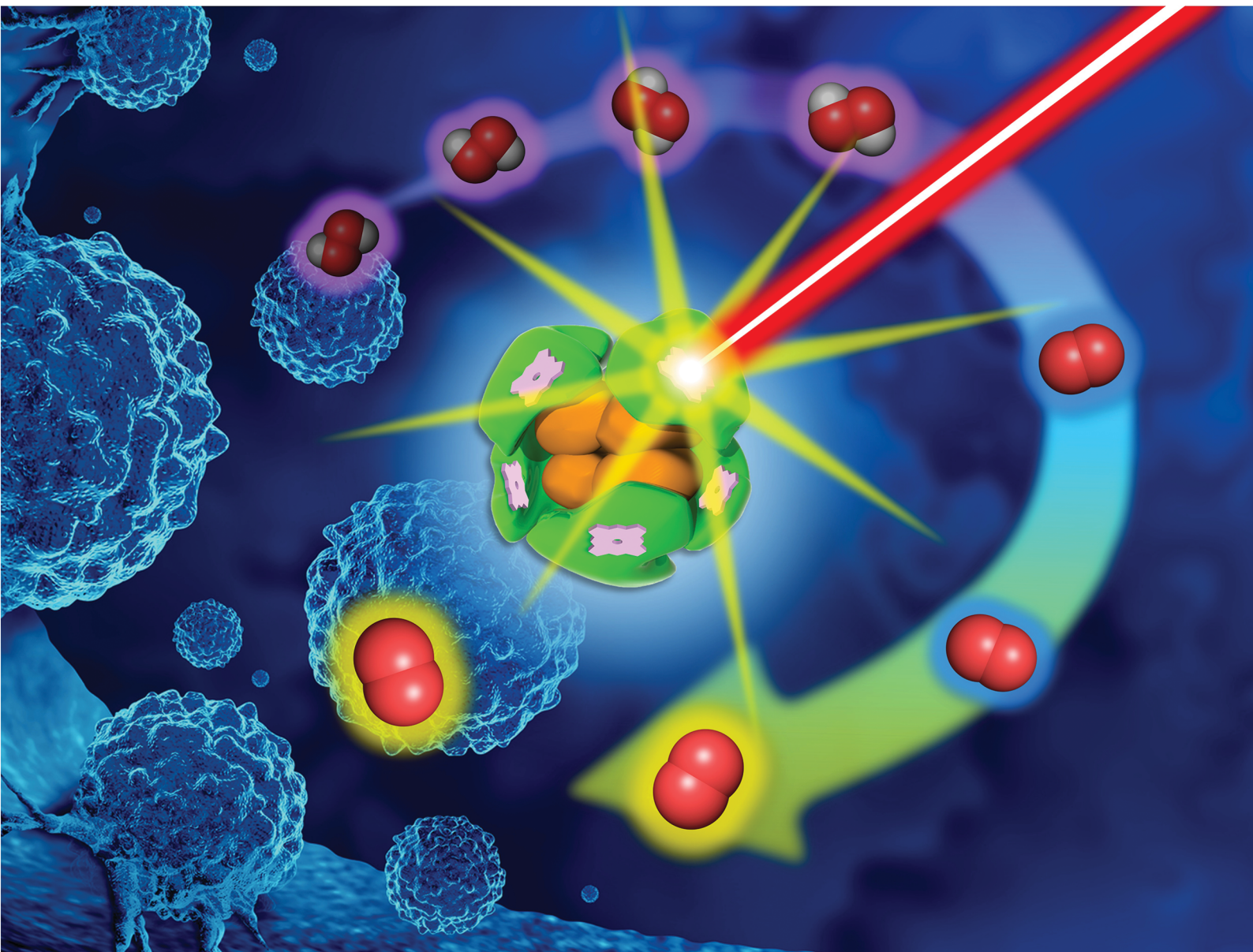


# Materials Advances

Volume 3  
Number 16  
21 August 2022  
Pages 6387–6658

[rsc.li/materials-advances](https://rsc.li/materials-advances)



ISSN 2633-5409


**PAPER**

Teruyuki Komatsu *et al.*  
Catalase-albumin cluster incorporating protoporphyrin IX: an O<sub>2</sub> generating photosensitizer for enhanced photodynamic therapy

## PAPER

[View Article Online](#)  
[View Journal](#) | [View Issue](#)Cite this: *Mater. Adv.*, 2022,  
3, 6451

# Catalase–albumin cluster incorporating protoporphyrin IX: an O<sub>2</sub> generating photosensitizer for enhanced photodynamic therapy†

Taiga Yamada, Maho Katsumi, Yuka Yagisawa, Masato Ichihara and Teruyuki Komatsu \*

Photodynamic therapy (PDT) is a non-invasive cancer treatment using reactive oxygen species (ROS) generated by light irradiation. An excited state photosensitizer produces active radicals (e.g. O<sub>2</sub><sup>•−</sup> and OH<sup>•</sup>) by electron transfer reactions (type I), while an excited triplet state photosensitizer generates singlet O<sub>2</sub> (<sup>1</sup>O<sub>2</sub>) by direct energy transfer to molecular O<sub>2</sub> (type II). This report describes the synthesis and PDT activity of the hemoprotein-based photosensitizer combined with O<sub>2</sub> production capability. Covalent wrapping of a catalase (Cat) with human serum albumins (HSAs) yielded the core–shell structured protein cluster Cat-HSA<sub>5</sub>, in which an average of five HSA molecules are bound to the Cat center. Cat-HSA<sub>5</sub> retained the high enzymatic activity of the hydrogen peroxide (H<sub>2</sub>O<sub>2</sub>) disproportionation reaction. Subsequently, the incorporation of protoporphyrin IX (PP) into an individual HSA unit resulted in a Cat-(HSA-PP)<sub>5</sub> cluster. The <sup>1</sup>O<sub>2</sub> generation ability of Cat-(HSA-PP)<sub>5</sub> was equivalent to that of the HSA-PP complex. Cytotoxicity with light irradiation was evaluated using HeLa cells. Cat-(HSA-PP)<sub>5</sub> demonstrated higher PDT activity than the HSA-PP complex. The Cat core provoked conversion of endogenous H<sub>2</sub>O<sub>2</sub> to O<sub>2</sub> efficiently in the cells to facilitate <sup>1</sup>O<sub>2</sub> formation in large amounts. Cat-(HSA-PP)<sub>5</sub> is a unique dual functional hemoprotein cluster (O<sub>2</sub> generation and photosensitization) that can achieve enhanced PDT.

Received 2nd March 2022,  
Accepted 17th June 2022

DOI: 10.1039/d2ma00242f

[rsc.li/materials-advances](https://rsc.li/materials-advances)

## Introduction

Photodynamic therapy (PDT) is a non-surgical cancer treatment using a light source such as an LED or laser.<sup>1–3</sup> A singlet oxygen (<sup>1</sup>O<sub>2</sub>) generated by energy transfer from a photosensitizing agent to O<sub>2</sub> is implicated as an intermediary species leading to cell death. However, hypoxia (pO<sub>2</sub> < 2.5 Torr) in a tumor microenvironment (TME)<sup>4</sup> inhibits the <sup>1</sup>O<sub>2</sub> formation and thereby restricts PDT.<sup>5</sup> Some investigators have reported the improvement of hypoxia in the TME using different means: (i) direct O<sub>2</sub>-transportation using an O<sub>2</sub> carrier,<sup>6</sup> (ii) *in situ* O<sub>2</sub>-generation by the disproportionation of endogenous H<sub>2</sub>O<sub>2</sub>

(50–100 μM),<sup>7</sup> and (iii) *in situ* O<sub>2</sub>-production by the splitting of H<sub>2</sub>O.<sup>8</sup> Cheng *et al.* reported that the perfluorocarbon-based O<sub>2</sub>-carrier including IR780 facilitates photodynamic activity.<sup>6</sup> Tae *et al.* demonstrated that graphene oxide with hemin and chlorin e6 becomes a useful reagent for PDT.<sup>9</sup> Photosensitizers must accumulate in the affected part. Generally, nanoparticles can access the tumor tissue closely by enhanced permeability and retention (EPR) effects.<sup>10,11</sup> Yan *et al.* reported that carrier free self-assembled nanoparticles based on chlorine e6 showed superior anticancer activity.<sup>12</sup> Using EPR effects, one can make nanoparticles to penetrate gaps in tumor blood vessels and to diffuse in the tissues (passive targeting).<sup>13</sup> Accumulation in tumors by passive targeting is, however, only 20–30% superior to that observed in normal tissues. Another technique is to use receptors that are overexpressed on tumors.<sup>13</sup> Immobilization of receptor binding ligands on the nanoparticle conferred high affinity with tumor tissues to the particles (active targeting).<sup>13</sup> For example, RGD peptides (arginylglycylaspartic acid) bind α<sub>v</sub>β<sub>3</sub> integrin on the vascular endothelial cell in the TME, which causes enhancement of cellular uptake.<sup>14</sup>

Earlier, we reported that Hb-HSA<sub>3</sub>, a core–shell protein cluster comprising hemoglobin (Hb) and human serum

Department of Applied Chemistry, Faculty of Science and Engineering, Chuo University, 1-13-27 Kasuga, Bunkyo-ku, Tokyo 112-8551, Japan.

E-mail: [komatsu@kc.chuo-u.ac.jp](mailto:komatsu@kc.chuo-u.ac.jp)

† Electronic supplementary information (ESI) available: Native-PAGE, SDS-PAGE and DLS of Cat-HSA<sub>5</sub>, Lineweaver–Burk plots of H<sub>2</sub>O<sub>2</sub> degradation using Cat-HSA<sub>5</sub>, time course of O<sub>2</sub> generated by H<sub>2</sub>O<sub>2</sub> dismutation using Cat-HSA<sub>5</sub>, absorption and fluorescence spectra of HSA-PP, fluorescence, transient absorption spectra and time course of the fluorescence intensity of Cat-(HSA-PP)<sub>5</sub>, and cell viability of HeLa cells treated with Cat-(HSA-PP)<sub>5</sub> without or with light irradiation. See DOI: <https://doi.org/10.1039/d2ma00242f>

albumins (HSAs), showed long circulation lifetime in the blood-stream as an artificial  $O_2$  carrier.<sup>15–17</sup> Several animal experiments have clarified their safety and efficacy as a red blood cell substitute.<sup>18–20</sup> The peripheral HSA units of Hb-HSA<sub>3</sub> can bind a wide range of hydrophobic compounds and drugs.<sup>21</sup> In fact, the incorporation of protoporphyrin IX (PP) into Hb-HSA<sub>3</sub> [Hb-(HSA-PP<sub>0.7</sub>)<sub>3</sub>] allowed adequate PDT activity to this cluster.<sup>22</sup> Furthermore, the Hb core brings  $O_2$  to the cell interior to accelerate the photodynamic properties. To our surprise, metHb-(HSA-PP<sub>0.7</sub>)<sub>3</sub> with a ferric Hb center showed higher PDT performance than the ferrous Hb-(HSA-PP<sub>0.7</sub>)<sub>3</sub>.<sup>22</sup> One possible explanation is that the  $H_2O_2$  disproportionation reaction by the metHb core improved hypoxia more efficiently than the  $O_2$ -transport by the Hb core. It is known that metHb exhibits weak peroxidase and catalase activities.<sup>23</sup> To confer stronger  $O_2$  generation ability to the cluster, a catalase (Cat), which is the most powerful  $H_2O_2$  dismutation enzyme in nature, should be exploited instead of a metHb core. For this study, we have demonstrated the synthesis, structure, and enzymatic activity of the Cat-HSA<sub>5</sub> cluster (Fig. 1). Moreover, the photophysical properties and PDT activity of Cat-HSA<sub>5</sub> incorporating PP [Cat-(HSA-PP)<sub>5</sub>, Fig. 1] have been characterized. The results indicate that our approach can create a new class of dual-functional hemoprotein-based medicines for advanced PDT.

## Results and discussion

### Synthesis of the Cat-HSA<sub>5</sub> cluster

Covalent wrapping of Cat with HSAs was achieved using a bifunctional cross-linking agent, *N*-succinimidyl 3-maleimido-propionate (SMP), which selectively connects a primary amine of Lys and sulfhydryl group of Cys (Fig. 1).<sup>17</sup> First, a total of 16 free Cys residues of Cat were blocked by *N*-ethyl maleimide (NEM).<sup>24</sup> The obtained Cat was reacted with SMP to prepare maleimide-activated Cat (MA-Cat). Second, the maleimide terminals of MA-Cat were coupled site-specifically with a Cys-34 of HSA. The cluster formation was confirmed using size exclusion chromatography (SEC) (Fig. 2(A)). The reaction mixture exhibited a new broad peak at the high molecular weight

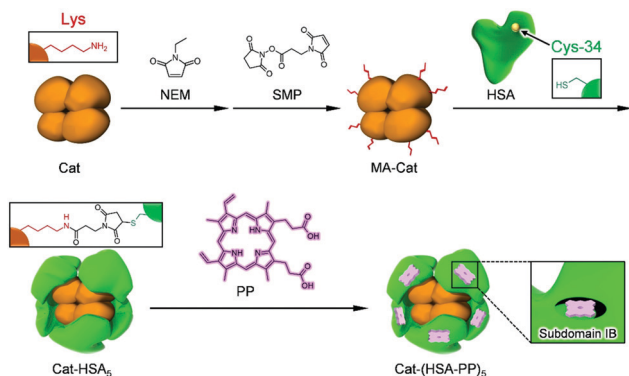


Fig. 1 Synthetic scheme of the Cat-HSA<sub>5</sub> cluster and Cat-(HSA-PP)<sub>5</sub> cluster.

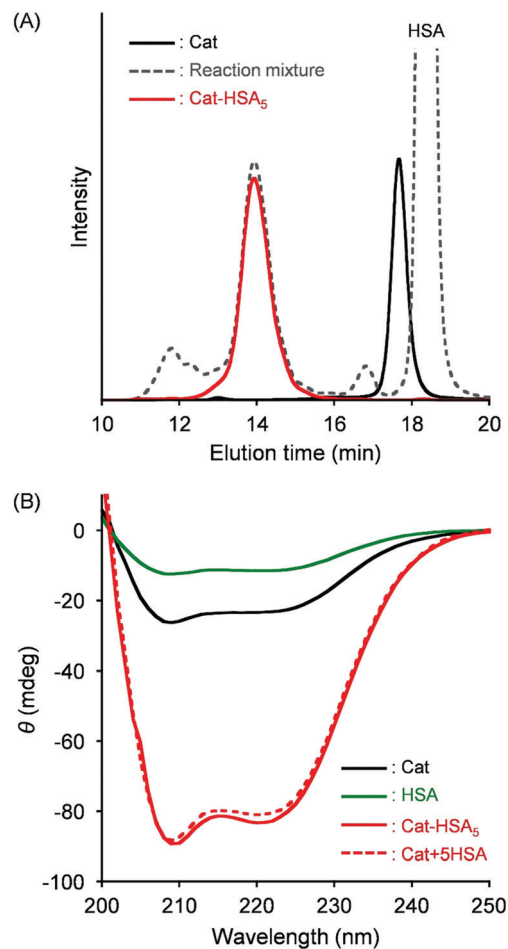


Fig. 2 (A) SEC profiles of the reaction mixture, Cat, and Cat-HSA<sub>5</sub>. (B) CD spectra of Cat-HSA<sub>5</sub>, Cat, and HSA (1  $\mu$ M) in PBS (pH 7.4) at 25  $^{\circ}$ C.

region (14 min), which could be Cat-HSA<sub>m</sub> derivatives. The unbound HSA was excluded using gel filtration chromatography (GPC) (yield: 70%) (Fig. 2(A)). The native-PAGE analysis of Cat-HSA<sub>m</sub> showed multiple bands (Fig. S1A, ESI<sup>†</sup>), suggesting that Cat-HSA<sub>m</sub> is a mixture of clusters with different HSA binding numbers. The SDS-PAGE analysis of Cat-HSA<sub>m</sub> also showed new bands at 112 kDa corresponding to a Cat unit (55 kDa) + 1HSA and at 176 kDa corresponding to a Cat unit + 2HSA (Fig. S1B, ESI<sup>†</sup>). From all these results of SEC, native-PAGE, and SDS-PAGE, we concluded that the HSA was covalently bound to the Cat core.

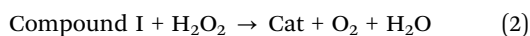
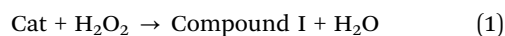
Based on assays of the total protein concentration and Cat concentration, the HSA/Cat ratio was found to be 5.0 (mol mol<sup>-1</sup>). The CD spectral pattern and intensity of Cat-HSA<sub>m</sub> coincided closely with the sum of the Hb spectrum and a five-fold enlarged HSA spectrum (Fig. 2(B)). These results indicated that (i) the average number of HSA units around the Cat is 5, and that (ii) the secondary structure of the individual protein component remains unaltered after the HSA conjugation. We designated this catalase-albumin cluster as Cat-HSA<sub>5</sub>. Subsequent DLS measurements showed that the diameter of Cat-HSA<sub>5</sub> (17.6 nm) is 1.3-fold greater than that of



Cat (13.6 nm) (Fig. S2, ESI†). A detailed inspection of the Cat-HSA<sub>5</sub> structure using transmission electron microscopy and scanning electron microscopy unfortunately failed, because the particle size of Cat-HSA<sub>5</sub> was too small to analyze. In general, nanomaterials with a diameter of less than 100 nm exhibited selective cytotoxicity because they penetrate tumor blood vessels as a result of the EPR effect.<sup>11</sup> Moreover, a 60 kDa glycoprotein (gp60) on the endothelial cell binds the HSA and takes the protein into the tumor by transcytosis.<sup>25</sup> Secreted protein acidic and rich in Cys (SPARC) overexpressed on various tumor tissues catches the HSA.<sup>26</sup> For these reasons, we expect that Cat-HSA<sub>5</sub> binds strongly to the tumor cells and that it is accumulated inside the cells. Apparently, the small particle size (approx. 18 nm) and plasma protein wrapping might be beneficial for both the enhanced EPR effect and active targeting that result in high accumulation in tumor tissues.

### Enzyme activity of the Cat-HSA<sub>5</sub> cluster

Cat decomposes H<sub>2</sub>O<sub>2</sub> into O<sub>2</sub> and H<sub>2</sub>O in a two-step reaction (2H<sub>2</sub>O<sub>2</sub> → O<sub>2</sub> + 2H<sub>2</sub>O).<sup>27</sup> First, the active site of heme reacts with H<sub>2</sub>O<sub>2</sub>, generating an oxoferryl porphyrin cation radical (Compound I) (eqn (1)). Subsequently, Compound I reacts with another H<sub>2</sub>O<sub>2</sub> to produce O<sub>2</sub> (eqn (2)).



Upon the addition of Cat-HSA<sub>5</sub> into H<sub>2</sub>O<sub>2</sub> solution, the absorbance at 240 nm decreased immediately, signaling the degradation of H<sub>2</sub>O<sub>2</sub>. The  $k_{\text{cat}}/K_{\text{m}}$  ( $k_{\text{cat}}$ , catalytic constant;  $K_{\text{m}}$ , Michaelis constant) value of Cat-HSA<sub>5</sub> was calculated using Lineweaver-Burk plots (Fig. S3, ESI†) as  $1.58 \times 10^7 \text{ M}^{-1} \text{ s}^{-1}$ , which was comparable with the value of Cat ( $1.57 \times 10^7 \text{ M}^{-1} \text{ s}^{-1}$ ). The amount of generated O<sub>2</sub> was also measured using a Clark-type O<sub>2</sub> electrode. After the addition of H<sub>2</sub>O<sub>2</sub> solution to the electrode chamber, the dissolved O<sub>2</sub> concentration increased gradually. The velocity of the O<sub>2</sub> generation was almost the same as that of H<sub>2</sub>O<sub>2</sub> degradation observed above. The rates of O<sub>2</sub> generation using Cat-HSA<sub>5</sub> and Cat were almost equal at each H<sub>2</sub>O<sub>2</sub> concentration (0.5–4.0 mM) (Fig. S4, ESI†). The  $k_{\text{cat}}/K_{\text{m}}$  value of Cat-HSA<sub>5</sub> was  $1.45 \times 10^7 \text{ M}^{-1} \text{ s}^{-1}$ , which closely resembled that of Cat ( $1.49 \times 10^7 \text{ M}^{-1} \text{ s}^{-1}$ ) and which agreed well with that obtained from the H<sub>2</sub>O<sub>2</sub> degradation. The enzyme activity of the Cat core was retained after the HSA binding. These observations suggest that the modification of Lys residues in Cat did not change the molecular environment around the prosthetic heme group. This result is consistent with the finding reported by Davis *et al.* that PEG-conjugated Cat and Cat possess almost equal catalytic activities.<sup>28</sup> We presume that Cat-HSA<sub>5</sub> can generate O<sub>2</sub> more efficiently than metHb-HSA<sub>3</sub> by the dismutation reaction of endogenous H<sub>2</sub>O<sub>2</sub> in TME because the catalytic activity of Cat-HSA<sub>5</sub> is much higher than that of metHb-HSA<sub>3</sub> ( $k_{\text{cat}}/K_{\text{m}} = 1.0 \times 10^2 \text{ M}^{-1} \text{ s}^{-1}$ ).<sup>22</sup>

### Photophysical properties of the Cat-(HSA-PP)<sub>5</sub> cluster

The HSA captures various insoluble endogenous and exogenous compounds. Common drug binding sites 1 and 2 are known to locate respectively in subdomains IIA and IIIA.<sup>21,29</sup> Many dyes can be used as photosensitizers for PDT. The most common currently used compounds are porphyrin derivatives. PP, a natural pigment, is bound strongly ( $K_{\text{a}}$ :  $\sim 10^5 \text{ M}^{-1}$ ) to the narrow D-shaped cavity in the subdomain IB of the HSA (drug binding site 3) and shows distinct absorption bands including a 630 nm band in the biological window.<sup>30</sup> In contrast, the aqueous solution of PP demonstrated the broadened split Soret band absorption ( $\lambda_{\text{max}}$ : 361, 441 nm) and no fluorescence emission (Fig. S5, ESI†). This finding is attributable to the fact that PP molecules form *J*-aggregate assemblies in water.<sup>31</sup> These characteristics differ greatly from the typical spectral shapes of the monomeric PP in the DMSO solution. It is noteworthy that the absorption and fluorescence spectral patterns of the HSA-PP complex and PP in DMSO are fundamentally the same as their general features (Fig. S5, ESI†), which implies that PP is monomolecularly bound within the HSA. The difference absorption spectrum of Cat-(HSA-PP)<sub>5</sub> minus Cat-HSA<sub>5</sub> coincided perfectly with the Soret and Q bands of HSA-PP (Fig. 3). We inferred that the five PP molecules are accommodated in the individual HSA shells of Cat-HSA<sub>5</sub>. In the GFC chromatogram of Cat-(HSA-PP)<sub>5</sub>, no peak of unbound PP was found. Consequently, Cat-(HSA-PP)<sub>5</sub> was exploited without further purification for the following photophysical and cytotoxicity experiments.

Cat-(HSA-PP)<sub>5</sub> showed a strong fluorescence of PP at 699 nm ( $\lambda_{\text{ex}}$ : 630 nm; Fig. S6A, ESI†). The intensity was slightly lower than that of HSA-PP because Cat-HSA<sub>5</sub> absorbs at 630 nm. The fluorescence intensity of Cat-(HSA-PP)<sub>5</sub> at 699 nm in PBS at 37 °C was almost unaltered during 7 days (Fig. S7, ESI†). Cat-(HSA-PP)<sub>5</sub> was sufficiently stable under physiological conditions. The transient absorption spectrum of Cat-(HSA-PP)<sub>5</sub> at 200 ns after laser flash photolysis exhibited a positive band at

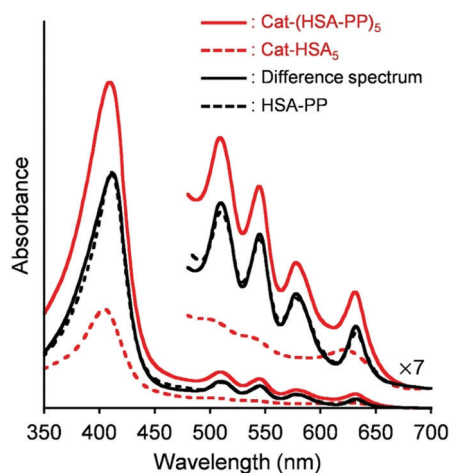


Fig. 3 Visible absorption difference spectrum of Cat-(HSA-PP)<sub>5</sub> ([Cat] = 4  $\mu\text{M}$ ) minus Cat-HSA<sub>5</sub> ([Cat] = 4  $\mu\text{M}$ ) and comparison with that of HSA-PP ([PP] = 20  $\mu\text{M}$ ) in PBS (pH 7.4) at 25 °C.



450 nm, which is based on the triplet-triplet (T-T) absorption of PP (Fig. S6B, ESI†). Concomitantly, the ground state bleaching of PP was also observable at 410 nm. The time dependence of the absorption decay was composed of a single-exponential profile. The spectral pattern and triplet lifetime ( $\tau_T = 0.96$  ms) were almost identical to those of HSA-PP ( $\tau_T = 0.90$  ms). Also, Hb-(HSA-PP)<sub>3</sub> and metHb-(HSA-PP)<sub>3</sub> respectively showed similar  $\tau_T$  values (0.87 ms and 0.92 ms).<sup>22</sup> All these results implied that electron transfer did not occur from the excited state of PP to the heme groups of the Cat core.

Next, the  $^1\text{O}_2$  generation ability of Cat-(HSA-PP)<sub>5</sub> was evaluated. The  $^1\text{O}_2$  formed by energy transfer from the excited photosensitizer to  $\text{O}_2$  leads to apoptosis of cells. The  $^1\text{O}_2$  scavenging reagent, ABDA, was used to detect  $^1\text{O}_2$ . Photoirradiation ( $\lambda > 620$  nm) of the photosensitizer solution containing ABDA caused bleaching at 380 nm, which is ascribed to ABDA oxidation.<sup>32,33</sup> This result supported the  $^1\text{O}_2$  formation by excited Cat-(HSA-PP)<sub>5</sub>. The reaction rate using Cat-(HSA-PP)<sub>5</sub> was almost identical to those obtained using HSA-PP, Hb-(HSA-PP)<sub>0.7</sub><sub>3</sub>, and metHb-(HSA-PP)<sub>0.7</sub><sub>3</sub> (Fig. 4).<sup>22</sup> Because the  $\tau_T$  value and  $^1\text{O}_2$  generation ability of each photosensitizer were comparable, the PDT activity is expected to be proportional to the  $\text{O}_2$  production ability in tumors.

#### PDT activity of the Cat-(HSA-PP)<sub>5</sub> cluster

Cytotoxicity and PDT activity were evaluated using HeLa cells. Cat-(HSA-PP)<sub>5</sub> and metHb-(HSA-PP)<sub>0.7</sub><sub>3</sub> can generate  $\text{O}_2$  by the enzymatic disproportionation reaction of endogenous  $\text{H}_2\text{O}_2$ . Although Hb-(HSA-PP)<sub>0.7</sub><sub>3</sub> can transport  $\text{O}_2$  directly into the cells, HSA-PP cannot supply  $\text{O}_2$ . Without light irradiation, the cell viability of each group was always beyond 90% irrespective of the PP concentration (0–3  $\mu\text{M}$ ) (Fig. 5(A)). The results of the present study show that the cytotoxicity of the four protein medicines was negligibly low under the dark condition. Moreover, the cytotoxicities of Cat-(HSA-PP)<sub>5</sub> and HSA-PP were evaluated under a wide range of PP concentrations

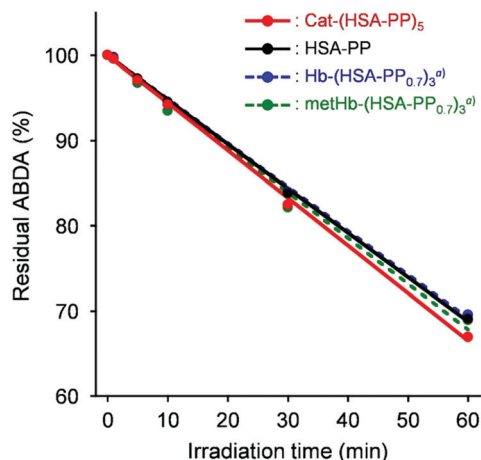


Fig. 4 Time courses of the residual ABDA percentage of Cat-(HSA-PP)<sub>5</sub>, HSA-PP, Hb-(HSA-PP)<sub>0.7</sub><sub>3</sub>, and metHb-(HSA-PP)<sub>0.7</sub><sub>3</sub> in PBS (pH 7.4) upon exposure to a LED lamp with a filter ( $\lambda > 620$  nm,  $25 \text{ mW cm}^{-2}$  at 630 nm).<sup>a</sup>Ref. 22.

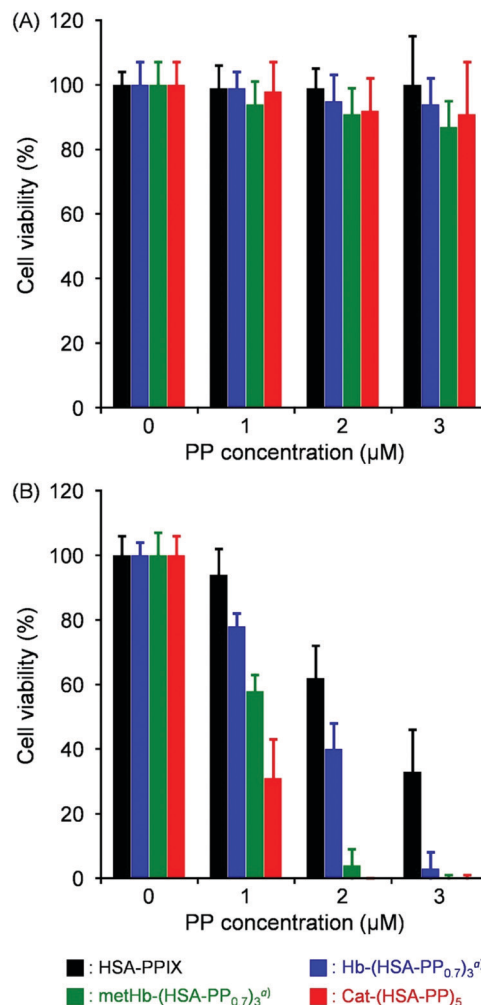


Fig. 5 Cell viability of HeLa cells exposed to Cat-(HSA-PP)<sub>5</sub>, HSA-PP, metHb-(HSA-PP)<sub>0.7</sub><sub>3</sub>, and Hb-(HSA-PP)<sub>0.7</sub><sub>3</sub>; (A) without light irradiation and (B) with light irradiation ( $\lambda > 620$  nm,  $25 \text{ mW cm}^{-2}$  at 630 nm, 5 min). Each value represents the mean  $\pm$  SD ( $n = 3$ ).<sup>a</sup>Ref. 22.

([PP] = 0–50  $\mu\text{M}$ ). The cell viability of Cat-(HSA-PP)<sub>5</sub> was slightly higher than that of HSA-PP (Fig. S8, ESI†). The half maximal inhibitory concentrations ( $\text{IC}_{50}$ ) of Cat-(HSA-PP)<sub>5</sub> and HSA-PP were ascertained as 47  $\mu\text{M}$  and 36  $\mu\text{M}$ , respectively. The cell viability decreased markedly by photoirradiation, dependent on the PP concentration (Fig. 5(B)). Microscopic observations of the HeLa cells after trypan blue staining also showed that light irradiation with Cat-(HSA-PP)<sub>5</sub> definitely induced cell death (Fig. S9, ESI†). This result implied that  $^1\text{O}_2$  was generated in the cells. Hb-(HSA-PP)<sub>0.7</sub><sub>3</sub> showed higher PDT activity than HSA-PP arising from  $\text{O}_2$  delivery by the Hb core. The  $\text{IC}_{50}$  value of Hb-(HSA-PP)<sub>0.7</sub><sub>3</sub> was ascertained as 1.8  $\mu\text{M}$  compared to 2.4  $\mu\text{M}$  of HSA-PP. It is particularly interesting that metHb-(HSA-PP)<sub>0.7</sub><sub>3</sub> showed further high photodynamic activity in comparison to Hb-(HSA-PP)<sub>0.7</sub><sub>3</sub>.<sup>22</sup> The amount of generated  $\text{O}_2$  by the  $\text{H}_2\text{O}_2$  disproportionation reaction with metHb in the cells is presumably greater than the transported  $\text{O}_2$  by Hb. As expected, Cat-(HSA-PP)<sub>5</sub> showed much greater PDT activity ( $\text{IC}_{50} = 0.7 \mu\text{M}$ ). In addition, we evaluated the PDT activities of

Cat-(HSA-PP)<sub>5</sub> and HSA-PP under hypoxic conditions ([O<sub>2</sub>] = 1%). Although the cell viability was higher than that under normoxic conditions ([O<sub>2</sub>] = 20%), Cat-(HSA-PP)<sub>5</sub> showed superior PDT activity compared to HSA-PP (Fig. S10, ESI†). We concluded that enzymatic O<sub>2</sub> formation by H<sub>2</sub>O<sub>2</sub> disproportionation in tumor cells was valid to promote PDT. Zhao *et al.* reported that hyaluronic acid-based nano-particles (approx. 200 nm) including Cat and chlorin e6 were accumulated efficiently in tumor tissues and that they acted as a good photosensitizer.<sup>34</sup> Hyaluronic acid is known to target the over-expressed CD44 receptor in several tumors. We expect that Cat-(HSA-PP)<sub>5</sub> with a diameter of approximately 18 nm and an HSA envelope would be beneficial both for its EPR effect and its active targeting to the tumor tissue *in vivo*.

## Conclusions

Simple covalent binding of HSAs to a Cat provided a core-shell structured Cat-HSA<sub>5</sub> cluster. The protein assay and CD spectrum revealed that the average binding number of HSAs to Cat was 5.0. The enzymatic activity of the Cat-HSA<sub>5</sub> cluster was maintained after HSA wrapping. Addition of PP into the aqueous Cat-HSA<sub>5</sub> solution enabled us to prepare the Cat-(HSA-PP)<sub>5</sub> complex. UV-vis absorption, fluorescence emission, and T-T absorption spectra proved that PPs were incorporated into the subdomain IB of the HSA entities in Cat-HSA<sub>5</sub>. The  $\tau_T$  and <sup>1</sup>O<sub>2</sub> generation ability of Cat-(HSA-PP)<sub>5</sub> were comparable to those of HSA-PP. As a consequence, Cat-(HSA-PP)<sub>5</sub> exhibited markedly high photodynamic activity compared to Hb-(HSA-PP<sub>0.7</sub>)<sub>3</sub> and methHb-(HSA-PP<sub>0.7</sub>)<sub>3</sub>. The superior H<sub>2</sub>O<sub>2</sub> dismutation ability of the Cat core unit to form O<sub>2</sub> allowed the peripheral HSA-PP photosensitizing units to enhance <sup>1</sup>O<sub>2</sub> production. Overall, our results have demonstrated Cat-(HSA-PP)<sub>5</sub> as a promising hemoprotein cluster with dual functionalities that can be of tremendous clinical importance as an O<sub>2</sub> generating photosensitizer.

## Experimental section

### Materials and apparatus

Bovine liver catalase (Cat), *N*-succinimidyl 3-maleimido-propionate (SMP), *N*-ethylmaleimide (NEM), antifoaming agent (Antifoam SI), hydrogen peroxide (H<sub>2</sub>O<sub>2</sub>), and 0.4 w/v% trypan blue were purchased from Fujifilm Wako Pure Chemical Corp. The human serum albumin (HSA) was purchased from Nihon Pharmaceutical Co., Ltd. Protoporphyrin IX (PP) and 9,10-anthracenediyl-bis(methylene) dimalonic acid (ABDA) were purchased from Merck KGaA. A Cell Counting Kit-8 (CCK-8) was purchased from Dojindo Laboratories. Other chemical reagents of special grade were used without further purification unless otherwise noted. The deionized water (18.2 MΩ cm) was prepared using a water purification system (Milli-Q IQ7003; Merck KGaA). UV-visible absorption spectra were recorded using a UV-visible absorption spectrophotometer (V-650; Jasco Corp. or UV-1900i; Shimadzu Corp.). Fluorescence emission spectra were obtained using a spectrofluorometer (FP-8300; Jasco Corp.).

SEC was conducted using a HPLC system (Prominence LC-20AD/CTO-20A/SPD-20A; Shimadzu Corp.) with an SEC column (YMC-Pack Diol-300 S-5; YMC Co. Ltd) using 50 mM PB (pH 7.4) as the mobile phase.

### Synthesis of the Cat-HSA<sub>5</sub> cluster

PBS solution (pH 7.4) of NEM (40 mM, 0.045 mL) was poured into Cat solution (30 μM, 2 mL, PBS). The mixture (NEM/Cat = 30, mol mol<sup>-1</sup>) was stirred under dark conditions for 1 hr at 25 °C. Then, the DMSO solution of SMP (18 mM, 0.2 mL) was added to the reactant (SMP/Cat = 60, mol mol<sup>-1</sup>). After stirring for 1 h, excess NEM and SMP were removed by gel filtration chromatography (GFC) using a desalting column (PD-10 Sephadex G-25; Cytiva). The collected solution of maleimide-activated Cat (MA-Cat) was concentrated to 2 mL ([Cat] = 30 μM) using a centrifugal filter device (Amicon ultra-15, 10 kDa MWCO; Merck KGaA) and was added gradually into the PBS solution of HSA (1.8 mM, 2.0 mL). The resultant (HSA/MA-Cat = 60, mol mol<sup>-1</sup>) was stirred gently under dark conditions for 18 hr at 4 °C. The obtained reaction mixture was subjected to GFC with Superdex 200 pg (Cytiva) to remove the unbound excess HSA. Based on the total protein assay using the protein assay kit (Pierce 660 nm; Thermo Fisher Scientific Inc.) and Cat assay using the UV-vis absorption spectrum ( $\epsilon_{405} = 2.5 \times 10^5 \text{ M}^{-1} \text{ cm}^{-1}$ ), the average HSA/Cat ratio of the product was calculated as 5.0. The obtained catalase-albumin cluster was designated as Cat-HSA<sub>5</sub>.

### CD and DLS measurements

Circular dichroism (CD) spectra were obtained using a spectropolarimeter (J-820; Jasco Corp.). A quartz cuvette (1 mm optical path length) was used for measurements of 200–250 nm. The molecular size of the cluster was ascertained from dynamic light scattering (DLS) measurements using a zetapotential and particle size analyzer (ELSZ-2000ZS; Otsuka Electronics Co., Ltd). The diameters were estimated from the particle-size distribution by the intensity. All measurements were taken at 25 °C.

### Enzyme activity of the Cat-HSA<sub>5</sub> cluster

The enzyme activity of Cat-HSA<sub>5</sub> was evaluated by measuring the H<sub>2</sub>O<sub>2</sub> degradation based on the absorption intensity at 240 nm. The PBS solution (pH 7.4) of Cat-HSA<sub>5</sub> (20 nM, 0.1 mL) was injected into H<sub>2</sub>O<sub>2</sub> solution (5.3 mM, 1.9 mL, PBS) in a quartz cuvette (10 mm optical path length). The absorbance change at 240 nm was monitored for 2 min. The same experiments were conducted at various H<sub>2</sub>O<sub>2</sub> concentrations (0–50 mM). The initial rate constant ( $\nu_0$ ) was calculated using the molar absorption coefficient of H<sub>2</sub>O<sub>2</sub> ( $\epsilon_{240} = 43.6 \text{ M}^{-1} \text{ cm}^{-1}$ ).<sup>35</sup> From the relationship between  $[\text{H}_2\text{O}_2]^{-1}$  and  $\nu_0^{-1}$  (Lineweaver-Burk plots), the catalytic activity ( $k_{\text{cat}}/K_m$ ) was ascertained. The control experiments were conducted using Cat (20 nM) under the same conditions. Furthermore, the catalytic activity of the Cat-HSA<sub>5</sub> was evaluated by monitoring the concentration of generated O<sub>2</sub> using an O<sub>2</sub>-monitoring system (Oxygraph; Hansatech Instruments Ltd). First, the PBS solution of



Cat-HSA<sub>5</sub> (1 nM, 0.98 mL containing 0.001% Antifoam SI) was poured into the electrode chamber. The dissolved O<sub>2</sub> was measured using gentle stirring under aerobic conditions at 25 °C. After confirming the O<sub>2</sub> concentration level constant, H<sub>2</sub>O<sub>2</sub> in PBS (25 mM, 20 µL) was added to adjust the H<sub>2</sub>O<sub>2</sub> concentration in the medium to 0.5 mM. Immediately after the addition of H<sub>2</sub>O<sub>2</sub>, an increase in the dissolved O<sub>2</sub> was observed. The same experiments were conducted using various H<sub>2</sub>O<sub>2</sub> concentrations (0–4 mM). The  $k_{\text{cat}}/K_{\text{m}}$  value of Cat-HSA<sub>5</sub> was determined from Lineweaver–Burk plots. The PBS solution of Cat (1 nM) was also measured in the same manner.

### Preparation of the Cat-(HSA-PP)<sub>5</sub> cluster

The DMSO solution of PP (2 mM, 0.02 mL) was injected slowly into the PBS solution (pH 7.4) of Cat-HSA<sub>5</sub> (4 µM, 1.98 mL). The obtained mixture was incubated for 3 hr with gentle stirring under dark conditions at 30 °C, yielding Cat-(HSA-PP)<sub>5</sub> (PP/Cat-HSA<sub>5</sub> = 5.0, mol mol<sup>−1</sup>). The UV-vis absorption spectrum revealed that PP is incorporated into the peripheral HSA moieties of Cat-HSA<sub>5</sub>. HSA-PP was also synthesized in the same manner.

### Laser flash photolysis

Transient absorption spectra and their time-course measurements were recorded using a time-resolved spectrophotometer (TSP-1000; Unisoku Co. Ltd) with a Q-switched Nd: YAG laser (Minilite ML II; Continuum Inc.), which generates a second-harmonic (532 nm) pulse of 5–7 ns duration (10 Hz). The PBS solution (pH 7.4) of Cat-(HSA-PP)<sub>5</sub> ([PP] = 3 or 10 µM) was held in a quartz cuvette (10 mm optical path length). For equilibration, N<sub>2</sub> gas was flowed into the sample cuvette for 2 h. The transient absorption spectra of the 3 µM solution were recorded at 25 °C. Time courses at 452 nm after laser flash photolysis of the 10 µM solution were measured at 25 °C. The triplet lifetime ( $\tau_{\text{T}}$ ) was determined using single exponential kinetics. The PBS solution of HSA-PP was also measured similarly.

### <sup>1</sup>O<sub>2</sub> generation measurement

The formation of <sup>1</sup>O<sub>2</sub> was detected using ABDA. The DMSO solution of ABDA was added to PBS solution (pH 7.4) of Cat-(HSA-PP)<sub>5</sub> ([PP] = 5 µM, [ABDA] = 50 µM, [DMSO] = 0.5 v/v%). The samples were light irradiated using a LED lamp (KTL-350; Kenko Tokina Corp.) equipped with an R-62 long pass filter ( $\lambda > 620$  nm; Hoya Corp.) (25 mW cm<sup>−2</sup> at 630 nm) with gentle stirring using a magnetic stirrer. After 1, 5, 10, 30, and 60 min irradiation, the UV-vis absorption spectra were recorded. From the decrease of the absorbance at 380 nm, the residual ABDA concentration was calculated. A sample without ABDA was prepared simultaneously in all cases; its absorption change at 380 nm was subtracted from the data of the sample solution with ABDA. The PBS solution of HSA-PP ([PP] = 5 µM, [ABDA] = 50 µM) was measured similarly.

### Evaluation of PDT activity

In a 5% CO<sub>2</sub>-95% air humidified incubator (MCO-5AC (UV); Sanyo Electric Co., Ltd), HeLa cells were grown at 37 °C in the

Dulbecco's Modified Eagle Medium (DMEM) supplemented with 10% fetal bovine serum (FBS), penicillin (100 unit per mL), streptomycin (100 unit per mL), and amphotericin B (0.25 µg mL<sup>−1</sup>). The HeLa cells were seeded into a 96-well plate (seeding density;  $7.5 \times 10^3$  cells per well in 100 µL) and were incubated at 37 °C for 24 h. Then, after 100 µL of photosensitizer [Cat-(HSA-PP)<sub>5</sub> or HSA-PP in DMEM, [PP] = 0–50 µM] was added to each well, and the cells were incubated at 37 °C in the dark for 4 hr under air ([O<sub>2</sub>] = 20%) or hypoxic conditions ([O<sub>2</sub>] = 1%) using a hypoxia culture kit (BIONIX; Sugiyama-Gen Co., Ltd). Subsequently, the cells were exposed to a LED lamp equipped with an R-62 long pass filter ( $\lambda > 620$  nm) (25 mW cm<sup>−2</sup> at 630 nm) for 5 min, followed by 20 hr incubation in the dark. After rinsing with PBS, 100 µL of the CCK-8 reagent diluted ten-fold with DMEM was added to each well. Then the cells were incubated for 1 h. Finally, the absorbance at 450 nm was measured using a microplate reader (Multiskan SkyHigh; Thermo Fisher Scientific Inc.).

The cell staining using trypan blue was conducted as follows. The supernatant in the well was carefully removed, followed by adding 100 µL of 0.4 w/v% trypan blue solution. After rinsing twice with 100 µL of PBS, optical microscopy observations were performed. The same experiments were also conducted without light irradiation.

## Author contributions

T. K. designed and initiated this study. All the authors conducted the experiments and analysed the data. T. Y. and T. K. drafted the manuscript.

## Conflicts of interest

There are no conflicts to declare.

## Acknowledgements

This work was supported by the Science Research Promotion Fund from Promotion and Mutual Aid Corporation for Private Schools of Japan, Grants-in-Aid for Scientific Research (B) (No. 21H01767) from JSPS, and a Joint Research Grant from the Institute of Science and Engineering, Chuo University.

## Notes and references

- 1 D. Dolmans, D. Fukumura and R. K. Jain, *Nat. Rev. Cancer*, 2003, **3**, 380–387.
- 2 Q. Zhang, J. He, W. Yu, Y. Li, Z. Liu, B. Zhou and Y. Liu, *RSC Med. Chem.*, 2020, **11**, 427–437.
- 3 X. Li, S. Lee and J. Yoon, *Chem. Soc. Rev.*, 2018, **47**, 1174–1188.
- 4 D. W. Zheng, B. Li, C. X. Li, J. X. Fan, Q. Lei, C. Li, Z. Xu and X. Z. Zhang, *ACS Nano*, 2016, **10**, 8715–8722.
- 5 L. Chen, S. F. Zhou, L. Su and J. Song, *ACS Nano*, 2019, **13**, 10887–10917.



- 6 Y. Cheng, H. Cheng, C. Jiang, X. Qiu, K. Wang, W. Huan, A. Yuan, J. Wu and Y. Hu, *Nat. Commun.*, 2015, **6**, 6–13.
- 7 Q. Chen, J. Chen, C. Liang, L. Feng, Z. Dong, X. Song, G. Song and Z. Liu, *J. Controlled Release*, 2017, **263**, 79–89.
- 8 L. Liu, Y. Zhang, W. Qiu, L. Zhang, F. Gao, B. Li, L. Xu, J. Fan, Z. Li and X. Zhang, *Small*, 2017, **13**, 1701621.
- 9 A. Sahu, K. Min, J. Jeon, H. S. Yang and G. Tae, *J. Controlled Release*, 2020, **326**, 442–454.
- 10 Y. Matsumura and H. Maeda, *Cancer Res.*, 1986, **46**, 6387–6392.
- 11 H. Cabral, Y. Matsumoto, K. Mizuno, Q. Chen, M. Murakami, M. Kimura, Y. Terada, M. R. Kano, K. Miyazono, M. Uesaka, N. Nishiyama and K. Kataoka, *Nat. Nanotechnol.*, 2011, **6**, 815–823.
- 12 R. Zhang, R. Xing, T. Jiao, K. Ma, C. Chen, G. Ma and X. Yan, *ACS Appl. Mater. Interfaces*, 2016, **8**, 13262–13269.
- 13 M. F. Attia, N. Anton, J. Wallyn, Z. Omran and T. F. Vandamme, *J. Pharm. Pharmacol.*, 2019, **71**, 1185–1198.
- 14 R. Haubner, W. A. Weber, A. J. Beer, E. Vabulienė, D. Reim, M. Sarbia, K. F. Becker, M. Goebel, R. Hein, H. J. Wester, H. Kessler and M. Schwaiger, *PLoS Med.*, 2005, **2**, 0244–0252.
- 15 D. Tomita, T. Kimura, H. Hosaka, Y. Daijima, R. Haruki, K. Ludwig, C. Böttcher and T. Komatsu, *Biomacromolecules*, 2013, **14**, 1816–1825.
- 16 Y. Morita, T. Yamada, M. Kureishi, K. Kihira and T. Komatsu, *J. Phys. Chem. B*, 2018, **122**, 12031–12039.
- 17 R. Funaki, T. Kashima, W. Okamoto, S. Sakata, Y. Morita, M. Sakata and T. Komatsu, *ACS Omega*, 2019, **4**, 3228–3233.
- 18 R. Haruki, T. Kimura, H. Iwasaki, K. Yamada, I. Kamiyama, M. Kohno, K. Taguchi, S. Nagao, T. Maruyama, M. Otagiri and T. Komatsu, *Sci. Rep.*, 2015, **5**, 1–9.
- 19 H. Iwasaki, K. Yokomaku, M. Kureishi, K. Igarashi, R. Hashimoto, M. Kohno, M. Iwazaki, R. Haruki, M. Akiyama, K. Asai, Y. Nakamura, R. Funaki, Y. Morita and T. Komatsu, *Artif. Cells, Nanomed., Biotechnol.*, 2018, **46**, S621–S629.
- 20 W. Okamoto, M. Hasegawa, T. Usui, T. Kashima, S. Sakata, T. Hamano, H. Onozawa, R. Hashimoto, M. Iwazaki, M. Kohno and T. Komatsu, *J. Biomed. Mater. Res.*, 2022, **110**, 1827–1838.
- 21 J. Ghuman, P. A. Zunszain, I. Petitpas, A. A. Bhattacharya, M. Otagiri and S. Curry, *J. Mol. Biol.*, 2005, **353**, 38–52.
- 22 T. Yamada and T. Komatsu, *ChemBioChem*, 2021, **22**, 2526–2529.
- 23 E. Nagababu and J. M. Rifkind, *Biochemistry*, 2000, **39**, 12503–12511.
- 24 W. A. Schroeder, J. R. Shelton, J. B. Shelton, B. Robberson, G. Apell, R. S. Fang and J. Bonaventura, *Arch. Biochem. Biophys.*, 1982, **214**, 397–421.
- 25 T. A. John, S. M. Vogel, C. Tiruppathi, A. B. Malik and R. D. Minshall, *Am. J. Physiol.*, 2003, **284**, 187–196.
- 26 A. Spada, J. Emami, J. A. Tuszyński and A. Lavasanifar, *Mol. Pharmacol.*, 2021, **18**, 1862–1894.
- 27 M. Alfonso-Prieto, X. Biarnés, P. Vidossich and C. Rovira, *J. Am. Chem. Soc.*, 2009, **131**, 11751–11761.
- 28 A. Abuchowski, J. R. McCoy, N. C. Palczuk, T. van Es and F. F. Davis, *J. Biol. Chem.*, 1977, **252**, 3582–3586.
- 29 P. A. Zunszain, J. Ghuman, T. Komatsu, E. Tsuchida and S. Curry, *BMC Struct. Biol.*, 2003, **3**, 1–9.
- 30 J. Hu, R. Allen, S. Rozinek and L. Brancaleon, *Photochem. Photobiol. Sci.*, 2017, **16**, 694–710.
- 31 J.-H. Fuhrhop, C. Demoulin, C. Böttcher, J. Köning and U. Siggel, *J. Am. Chem. Soc.*, 1992, **114**, 4159–4165.
- 32 N. A. Kuznetsova, N. S. Gretsova, O. A. Yuzhakova, V. M. Negrimovskii, O. L. Kaliya and E. Luk'yanets, *Russ. J. Gen. Chem.*, 2001, **71**, 36–41.
- 33 S. Wang, F. Yuan, K. Chen, G. Chen, K. Tu, H. Wang and L. Q. Wang, *Biomacromolecules*, 2015, **16**, 2693–2700.
- 34 S. Z. F. Phua, G. Yang, W. Q. Lim, A. Verma, H. Chen, T. Thanabalu and Y. Zhao, *ACS Nano*, 2019, **13**, 4742–4751.
- 35 I. Hara, N. Ichise, K. Kojima, H. Kondo, S. Ohgiya, H. Matsuyama and I. Yumoto, *Biochemistry*, 2007, **46**, 11–22.

